ACS APPLIED MATERIALS & INTERFACES

Research Article

www.acsami.org

Iron Insertion and Hematite Segregation on Fe-Doped TiO_2 Nanoparticles Obtained from Sol–Gel and Hydrothermal Methods

Reginaldo da S. Santos,[†] Guilherme A. Faria,[‡] Carlos Giles,[‡] Carlos A. P. Leite,[‡] Herbert de S. Barbosa,[†] Marco A. Z. Arruda,[†] and Claudia Longo*[,†]

[†]Institute of Chemistry, University of Campinas – UNICAMP, PO box 6154, 13083-970, Campinas, SP, Brazil and

[‡]Institute of Physics "Gleb Wataghin", University of Campinas – UNICAMP, 13083-970, Campinas, SP, Brazil

Supporting Information

ABSTRACT: Iron-doped TiO_2 (Fe:TiO_2) nanoparticles were synthesized by the sol–gel method (with Fe/Ti molar ratio corresponding to 1, 3, and 5%), followed by hydrothermal treatment, drying, and annealing. A similar methodology was used to synthesize TiO_2 and α-Fe_2O_3 nanoparticles. For comparison, a mixture hematite/titania, with Fe/Ti = 4% was also investigated. Characterization of the samples using Rietveld refinement of X-ray diffraction data revealed that TiO_2 consisted of 82% anatase and 18% brookite; for Fe:TiO_2, brookite increased to 30% and hematite was also identified (0.5, 1.0, and 1.2 wt % for samples prepared with 1, 3, and 5% of Fe/Ti). For hematite/titania mixture, Fe/Ti was estimated as 4.4%, indicating the Rietveld method reliability for estimation of phase composition. Because the band gap energy, estimated as 3.2 eV for TiO_2, gradually ranged from 3.0 to 2.7 eV with increasing Fe content at Fe:TiO_2, it can be assumed that a Fe fraction was also inserted as dopant in the TiO_2 lattice. Extended X-ray absorption fine structure spectra obtained for the Ti K-edge and Fe K-edge indicated that absorbing Fe occupied a Ti site in the TiO_2 lattice, but hematite features were not observed. Hematite particles also could not be identified in the images obtained by transmission electron microscopy, in spite of iron identification by elemental mapping, suggesting that hematite can be segregated at the grain boundaries of Fe:TiO_2.

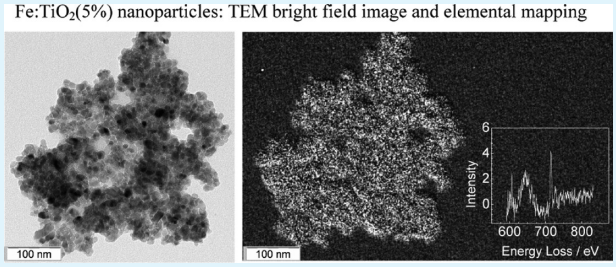

KEYWORDS: *Fe-doped TiO_2, sol–gel method, Rietveld refinement, phase segregation, EXAFS*

1. INTRODUCTION

TiO_2 is a semiconductor largely used as photocatalyst for solar energy conversion because of its relative low cost and excellent chemical stability.[1] TiO_2 deposited as a porous thin film on a conductive substrate allows its application as photoanode in dye-sensitized TiO_2 solar cells,[2−6] and in photoelectrochemical cells for water splitting[7] or for oxidation of organic pollutants.[8−10] Recently, we reported a successful system that mineralized phenol by electroassisted photocatalysis using porous TiO_2 electrodes connected to a solar cell, in an efficient and inexpensive method to achieve water remediation.[9]

Solar energy conversion results from the electron/hole separation that can occur under irradiation; however, the wide band gap energy (E_{BG} = 3.2 eV for anatase phase) limits the TiO_2 photoactivity to UV irradiation (380 nm), that corresponds to less than 5% of sunlight.[1,10] The TiO_2 light harvesting can be enhanced by sensitization with adsorbed nanoparticles of a smaller band gap semiconductor, or by doping with metallic or nonmetallic elements.[11−16]

Iron has been considered a good candidate for TiO_2 doping due to the Fe^{3+} and Ti^{4+} ionic radii similarity;[17] Fe doped TiO_2 (Fe:TiO_2) can be easily prepared by the sol–gel method, with controlled crystalline phase and particle size.[10,18−20] Compared to nondoped TiO_2 samples (as electrodes or suspended particles), Fe:TiO_2 always exhibited enhanced light harvesting; however, controversial results can be found for its performance as photocatalyst. Whereas some studies reported that iron doping in TiO_2 resulted in higher activity for photocatalytic oxidation of phenol,[20] and dyes such as methylene blue[11,12,19] or methyl orange,[21] others described lower activity for degradation of alcohols,[22,23] and methylene blue[11] or Rhodamine B dyes.[24]

Probably, the Fe:TiO_2 photocalyst activity strongly depends on the structural modifications associated to iron incorporation as dopant (interstitial or substitutional) and a possible hematite (α-Fe_2O_3) phase segregation. Since hematite exhibits a much lower dielectric constant when compared to TiO_2,[25] the hematite presence can affect the separation of photogenerated charges and the photocatalytic activity. Hematite segregation can occur when the iron concentration exceeds the limit that can be accommodated into the TiO_2 lattice, and again, controversial results were found in the literature and depended on the synthesis procedure. It was already stated, for instance, that hematite segregation was observed just for Fe:TiO_2

Received: July 24, 2012
Accepted: September 28, 2012
Published: September 28, 2012

   dx.doi.org/10.1021/am301444k | ACS Appl. Mater. Interfaces 2012, 4, 5555−5561

prepared with relative Fe/Ti content higher than 20 wt % in the precursors and after annealing at 600 °C;[26] however, the segregation of hematite, as well as Fe_2TiO_5, was also observed for much lower Fe concentrations, such as 1 at % for Fe:TiO_2 synthesized by the sol−gel method.[27,28]

Motivated to contribute for a better understanding of the effects of iron insertion and hematite segregation in Fe:TiO_2 photocatalysts, we investigated the morphological and structural properties of nanosized particles of TiO_2, Fe:TiO_2 (with Fe/Ti molar ratio corresponding to 1, 3, and 5%) and a mixture TiO_2/α-Fe_2O_3 (with Fe/Ti = 4%) by X-ray diffraction (XRD) analyzed by Rietveld refinement, extended X-ray absorption fine structure (EXAFS) and other surface analysis techniques.

2. EXPERIMENTAL SECTION

2.1. Synthesis of TiO_2, Fe:TiO_2, and α-Fe_2O_3 Aqueous Suspensions. Titanium tetra-isopropoxide, TTIP, (Aldrich-97%), $Fe(NO_3)_3{\cdot}9H_2O$ (Vetec-99%), nitric acid (Merck-65%) and all other chemicals were of P.A. grade and used without any further purification. Deionized water from a Milli-Q water purification system was used throughout the work. The α-Fe_2O_3 sample was prepared from 0.01 mol L^{-1} of $Fe(NO_3)_3$ aqueous solution maintained at 96 °C for 24 h;[29] after being cooled at room temperature, an orange-red suspension was obtained. Fe:TiO_2 samples were synthesized by sol−gel method followed by hydrothermal treatment, using precursors with the Fe/Ti nominal molar ratio corresponding to 1, 3 and 5%; these samples are respectively identified as Fe:TiO_2(1%), Fe:TiO_2(3%) and Fe:TiO_2(5%). For comparison, a TiO_2 sample was also prepared using the same procedure and without $Fe(NO_3)_3$. Under vigorous stirring, 2.5 mL of TTIP (that contained 0.39 g of Ti) was added to 30 mL of aqueous $Fe(NO_3)_3$ and HNO_3 solution (pH ∼1.3), resulting in the instantaneous formation of a pale yellow precipitate. This suspension was peptized at 85 °C under stirring for 12 h (for dispersion of agglomerates into primary particles), filtered using a glass frit, and then transferred into a Teflon lined stainless steel autoclave, which was sealed and heated at (200 ± 5) °C for 8 h. After being cooled at room temperature, the autoclave was opened and an aliquot of the supernatant (7 mL) was carefully collected for analysis; the residual aqueous suspension was then dispersed by ultrasonic bath for 30 min. The suspension of each sample was concentrated using a rotary evaporator (at low pressure, 50 °C) for achieving ca. 15 wt % for the final oxide concentration and then transferred to a closed flask, for posterior preparation of powders. For each sample, the aliquot of the supernatant solution was later analyzed by inductively couple plasma optical emission spectroscopy (ICP OES), using the Perkin-Elmer Optical 3000 DV equipment, in order to determine the concentration of Fe and Ti that remained in the solution after the hydrothermal treatment.

2.2. Preparation and Characterization of Oxide Powders. A small aliquot of the aqueous suspension of each oxide was first dried in oven at 60 °C and the resulting powder was crushed employing an agate set of mortar and pestle. The sample was heated in an oven from ambient temperature (10 °C/min), maintained at 350 °C for 30 min and then at 450 °C for 30 min; after cooling down to ambient temperature, the sample was crushed again. This procedure was also used to prepare the TiO_2/α-Fe_2O_3 (with Fe/Ti = 4%) mixture. The specific surface areas were determined by Brunauer−Emmett−Teller (BET) method from Nitrogen adsorption at 77 K (Quantachrome Nova 4200e equipment). The band gap energy for each sample was estimated by a modified Kubelka−Munk function,[30] from UV−vis diffuse reflectance spectra (UV−vis DRS), taken with a Teflon disk as the reference standard (Cary 5G-Varian apparatus, equipped with an integrating sphere). The total Ti and Fe concentrations in two sets of annealed samples were estimated by ICP OES after microwave-assisted acid decomposition (details were described as the Supporting Information). Examination by transmission electron microscopy (TEM) was performed for samples of the annealed particles resuspended in water (ca. 13 ng L^{-1}), using a Carl Zeiss CEM-902 equipment; electron energy-loss spectroscopy (EELS) and elemental mapping were also obtained (Carl Zeiss Libra-120 TEM microscopy).

XRD and Rietveld Refinement. XRD analysis were taken at room temperature using a Rigaku Rint-2000 equipment with a CuKα, λ = 1.5406 Å radiation, from $10° \leq 2\theta \leq 90°$, with a 0.02° step size and 5 s per point. The instrumental broadening was checked with a crystalline standard NIST LaB_6 powdered sample. Diffraction peaks of crystalline phases were compared with those of standard compounds reported in the Joint Committee on Powder Diffraction Standards (JCPDS) database. Rietveld refinement was accomplished using GSAS-EXPGUI software package;[31,32] the phase composition for the samples was estimated considering the contribution of anatase (space group *I*41/*amdZ* (141)), brookite (space group *Pbca* (61)) and hematite (space group $R\bar{3}c$ (167)).[26,33] Fittings were performed using pseudo-Voigt functions and evaluated in terms of the weighted and expected factors (R_{wp}, R_{ex}), and their ratio, which corresponds to the goodness-of-fit (χ^2).[34]

EXAFS Local Structure Investigation. X-ray absorption spectra were collected at the Brazilian Synchrotron Light Laboratory (LNLS), station D08B-XAFS2, at room temperature (ca. 25 °C), using a Si (111) monochromator. The samples were pressed into pellets of suitable thickness; metallic Fe and Ti foils were also measured, as reference. Ti K-edge (4850 to 5700 eV) and Fe K-edge (7000 to 7750 eV) spectra were collected in the transmission mode; the average of three scans was considered for each sample. The data were analyzed by Athena in IFEFFIT software package; normalized EXAFS oscillations as a function of the photoelectron wavenumber (χ(k)) were obtained using standard procedures, considering the pre-edge and postedge smooth backgrounds from the absorption spectra. The Fourier Transforms (FT) of the k^2 ($\chi(k)$) spectra were associated to the radial distribution around the absorbing Ti (or Fe) atoms.

3. RESULTS AND DISCUSSION

3.1. Characterization of TiO_2, Fe:TiO_2, and α-Fe_2O_3/TiO_2 Powder Samples. Hydrolysis of TTIP followed by hydrothermal treatment resulted in quantitative precipitation as TiO_2; from ICP OES analysis, the total amount of remaining Ti in the supernatant ranged from 0.1 to 0.7 mg, which corresponds up to 0.2% of the initial quantity added as TTIP. For the supernatant solutions collected from the Fe:TiO_2 samples preparation, the Fe amount ranged from 0.03 to 0.1 mg, less than 2% of the $Fe(NO_3)_3$ introduced as precursor. The higher remaining iron concentration can be associated to the larger hematite solubility, when compared to TiO_2.[35] The final Ti and Fe concentrations in annealed TiO_2 and Fe:TiO_2 powder samples were also estimated by ICP OES after microwave-assisted acid decomposition (Table 1). Considering the nominal values, the measured Ti concentrations in the samples differed by less than 10% of the expected amounts; higher discrepancies were found for Fe (ranging from 10 to 20%), probably because of its smaller relative concentrations in the samples.

Table 1. Titanium and Iron Concentrations Estimated by ICP OES for Two Sets of Annealed TiO_2 and Fe:TiO_2 samples

	nominal concentration (mmol g^{-1})		measured concentration (mmol g^{-1})	
sample	C_{Fe}	C_{Ti}	C_{Fe}	C_{Ti}
TiO_2		12.5		12.0; 11.9
Fe:TiO_2(1%)	0.13	12.4	0.13; 0.12	12.5; 12.4
Fe:TiO_2(3%)	0.38	12.2	0.32; 0.31	11.2; 11.9
Fe:TiO_2(5%)	0.63	11.9	0.51; 0.50	11.3; 11.9

dx.doi.org/10.1021/am301444k | ACS Appl. Mater. Interfaces 2012, 4, 5555−5561

After annealing at 450 °C, the resulting powder exhibited different colors; while the nondoped TiO_2 was white, the Fe:TiO_2 changed from pale yellow to orange on increasing the relative iron content. However, examination by scanning electron microscopy or by TEM revealed similar morphology for all the samples. Figure 1 shows a TEM image obtained for

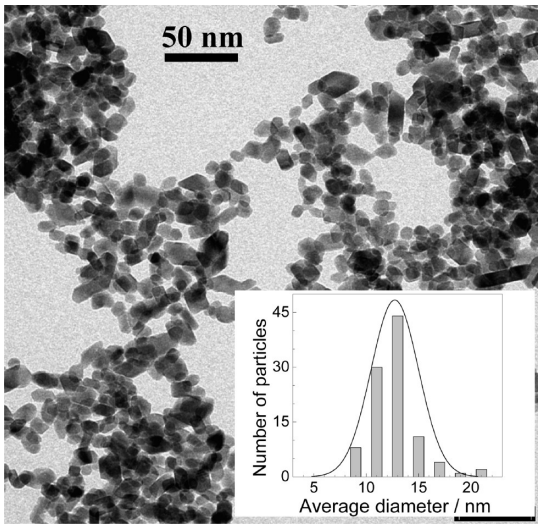

Figure 1. TEM image of annealed Fe:TiO_2(5%) sample. Inset: distribution of the average diameter obtained from a set of one hundred particles.

the Fe:TiO_2(5%) sample; the histogram of the average diameter estimated from a set of one hundred particles, presented as inset, revealed that the average diameter ranged from 10 to 23 nm, and corresponds to 13 nm for most of the particles.

Table 2 presents the surface area and pore volume determined for annealed powder samples from N_2 adsorption−desorption curves. Type IV isotherms were obtained (data not shown), suggesting mesoporous structure. Compared to TiO_2, doped Fe:TiO_2 exhibited higher surface area and smaller pore volume.

Table 2. Surface Area and Pore Volume Estimated from BET N_2 Adsorption−Desorption Isotherms for TiO_2 and Fe:TiO_2 Powder Samples

sample	surface area (m^2 g^{-1})	pore volume (cm^3 g^{-1})
TiO_2	94	0.22
Fe:TiO_2(1%)	114	0.26
Fe:TiO_2(3%)	122	0.30
Fe:TiO_2(5%)	122	0.28

Figure 2 exhibits the XRD patterns for annealed TiO_2 and Fe:TiO_2 powders; crystalline samples were obtained, consisting of anatase (JCPDS 21−1272) and brookite (JCPDS 29−1360) phases. Also, hematite phase (JCPDS 33−0664) can be identified in the samples prepared with 3 and 5% of Fe/Ti molar ratio, indicating phase segregation of α-Fe_2O_3. In fact, this synthesis procedure provided crystalline nanosized particles even before the annealing procedure; XRD measurements performed after peptization (12 h at 85 °C) already revealed the characteristic reflections peaks for the anatase and brookite phases (see Figure S1 in the Supporting Information), which were intensified as a consequence of the hydrothermal

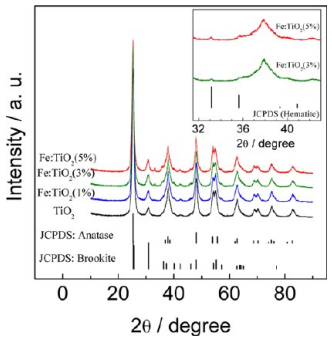

Figure 2. XRD patterns for annealed TiO_2 and Fe:TiO_2 powder samples prepared with different Fe/Ti molar ratio. Inset: detail of hematite peaks observed in Fe:TiO_2(3%) and Fe:TiO_2(5%) samples.

treatment (8 h at 200 °C in autoclave) and annealing (350 °C for 30 min, 450 °C for 30 min).

The phase composition for each annealed sample was estimated by Rietveld refinement, taking into account the contribution of anatase, brookite and hematite phases. The relative phase composition, i.e., the fraction for each phase, in weight (W_p, in wt %), can be estimated considering the mass of the unit cell for every p phase (m_p) and the individual scale factor (S_p) determined from Rietveld method, according to the eq 1

$$W_p = \frac{S_p m_p}{\sum_{i=1} (S_i m_i)} \quad (1)$$

First, the Rietveld refinement was used to analyze the XRD data for a mixture prepared with annealed powders of α-Fe_2O_3 and TiO_2, with Fe/Ti = 4.0 wt %. Figure 3 shows the XRD pattern

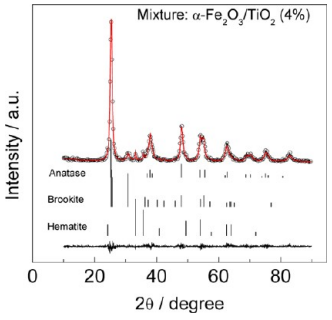

Figure 3. XRD data (symbols) and respective Rietveld refinement (solid line) for a mixture of TiO_2 and α-Fe_2O_3 (Fe/Ti = 4%) annealed powders. The Bragg reflections for anatase, brookite, and hematite phases (vertical bars) and the curves for the difference between experimental data and calculated profiles were also indicated.

(symbols) and the respective Rietveld refinement (solid lines) obtained for the mixture, as well as the Bragg reflections for anatase, brookite and hematite phases (vertical bars). The obtained Rietveld refinement exhibited good agreement with the experimental data (R_{wp} = 7.9% and R_{ex} = 6.9%, thus χ^2 =1.14), as observed in the curve for their difference. The hematite relative concentration was estimated as 4.4 wt %, indicating the reliability of the Rietveld method for a quantitative determination of phase composition in these samples.

Figure 4 shows the experimental data and the respective refinement for the TiO_2 and Fe:TiO_2(5%) annealed powders

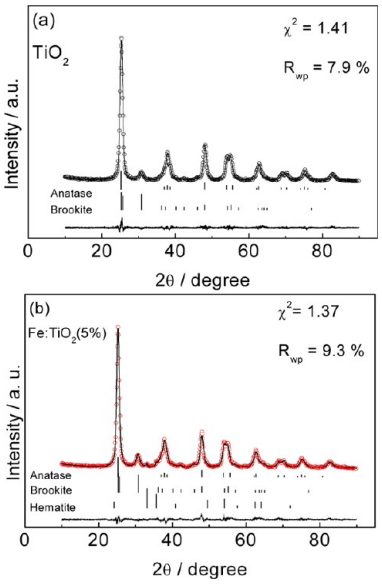

Figure 4. XRD data (symbols) and respective Rietveld refinement (solid lines) for (a) TiO_2 and (b) Fe:TiO_2(5%) annealed powders. The Bragg reflections for the anatase, brookite, and hematite phases (vertical bars) and the curves for the difference between experimental data and calculated profiles are also indicated.

(χ^2 corresponding to ca. 1.4); similar results were observed for other samples. The phase composition and lattice parameters estimated by Rietveld refinement are presented in Table 3.

The estimated parameters revealed that anatase is the major crystalline phase in these oxides and the brookite contribution, estimated as 18% for TiO_2, increased for the Fe:TiO_2 samples. Also, hematite was identified in all the samples prepared in the presence of $Fe(NO_3)_3$, and its weight fraction systematically augmented from 0.5 to 1.2 wt % when the Fe concentration in the precursors increased from 1.0 to 5.0%. Compared to nondoped TiO_2, for the Fe:TiO_2(1%) sample a higher contribution of brookite (32.0 wt %) and the segregation of hematite (0.5 wt %) were found; also, the lattice parameters and unit cell volumes for anatase and brookite phases were enlarged (see the Supporting Information, Figure S2). The presence of iron increased these lattice parameters probably owing to the larger ionic radius of Fe^{3+} (0.645 Å) in comparison to the Ti^{4+} ion (0.604 Å).[36] However, the lattice parameter evolutions differed for the anatase and brookite phases (see the Supporting Information, Figure S2a, b, respectively). The lattice parameter variations for the brookite phase were not regular, whereas for anatase, both *c* and *a* lattice parameters changed proportionally. Thus, because for the anatase phase the *c*/*a* ratio corresponded to 2.505 for all the samples (see Figure S2c in the Supporting Information), it can be concluded that the iron insertion caused a regular lattice expansion into its a- and *c*-axis, as already discussed for S-doped TiO_2.[37] Also, the lattice parameters and unit cell volume of brookite were more affected than their respective values estimated for anatase, indicating that iron could have been preferentially inserted into the brookite phase. For the sample prepared with precursors containing 3% of Fe/Ti, brookite and hematite phases corresponded to 35.8 and 1.0 wt %, respectively. The lattice parameter variations for brookite were not regular, while for the anatase phase these values and the unit-cell volume decreased and were similar to those estimated for the nondoped TiO_2. Maybe, in this condition, hematite segregation and iron insertion into brookite phase were more favorable than in the anatase phase. Finally, for the Fe:TiO_2(5%) sample, the brookite and hematite contributions corresponded to 30.7 and 1.2 wt %, respectively. Furthermore, the lattice parameters and the unit cell volume increased, and these effects were more significant for brookite in comparison to anatase. Thus, the results obtained from the Rietveld refinement of XRD data indicated that part of the iron segregated as α-Fe_2O_3, while another fraction was incorporated as dopant into the TiO_2 lattice. This hypothesis can be supported considering the differences in the color and absorption of the Fe:TiO_2 samples when compared to the one for TiO_2 and to the α-Fe_2O_3/TiO_2 mixture (Figure 5).

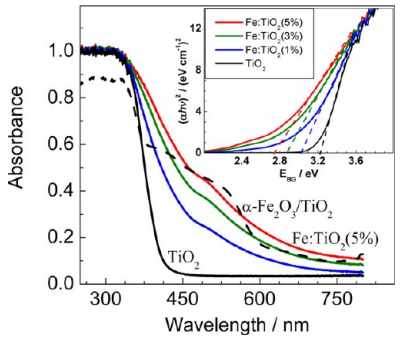

Figure 5. UV−vis diffuse reflectance spectra for TiO_2, Fe:TiO_2, and the α-Fe_2O_3/TiO_2 mixture (dotted line). Inset: the respective Kubelka−Munk function for estimating the band gap energy (E_{BG}) from variation of $(\alpha h\nu)^2$ with photon energy ($h\nu$).

For TiO_2, a white powder, the absorption onset is observed at ca. 380 nm. For the Fe:TiO_2 samples, the color gradually changed from pale yellow to orange with increasing iron content, whereas the onset of absorption also shifted toward the visible-light region; the red shift in the absorption spectra can be associated to the band gap narrowing of these semiconductors. A very different UV−vis DRS spectrum was obtained for the α-Fe_2O_3/TiO_2 mixture (dotted line). Thus,

Table 3. Phase Composition and Lattice Parameters Estimated from XRD Data Using Rietveld Refinement[†]

		lattice parameters (Å)				
		anatase		brookite		
sample	phase composition* (wt %) Ana:Bro:Hem	*a* = *b*	*c*	*a*	*b*	*c*
TiO_2	82.0:18.0: 0.0	3.782(6)	9.474(8)	9.170(2)	5.441(2)	5.174(5)
Fe:TiO_2(1%)	67.5:32.0:0.5	3.784(5)	9.479(3)	9.184(6)	5.438(3)	5.178(9)
Fe:TiO_2(3%)	63.2:35.8:1.0	3.782(5)	9.473(1)	9.150(2)	5.449(9)	5.179(0)
Fe:TiO_2 (5%)	68.1:30.7:1.2	3.788(2)	9.488(1)	9.269(2)	5.468(1)	5.172(5)

[†]Rietveld refinement parameters: R_{wp} = 8.6 ± 0.7% and χ^2 = 1.4 ± 0.1 *Ana = anatase, Bro = brookite, and Hem = hematite phases.

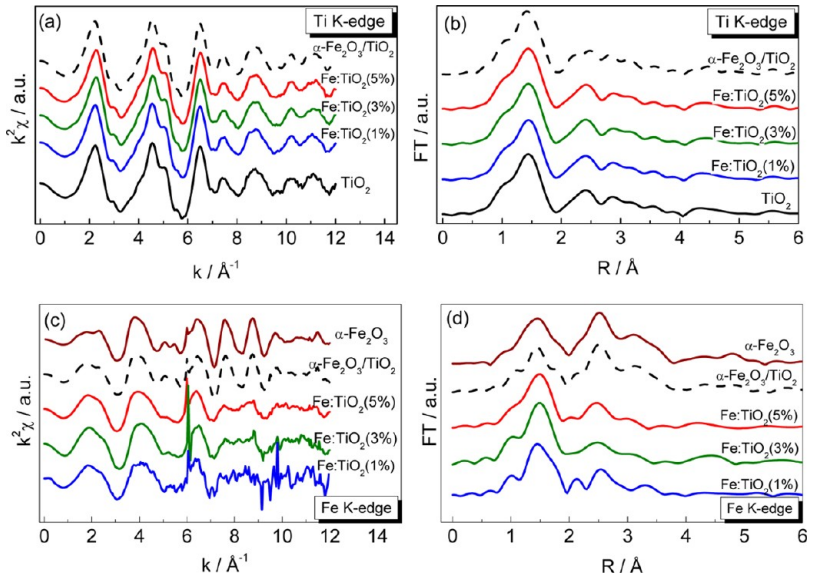

Figure 6. (a, c) EXAFS spectra, and (b, d) corresponding Fourier transforms for annealed powder samples of TiO_2, α-Fe_2O_3, Fe:TiO_2, and α-Fe_2O_3/TiO_2 (Fe/Ti = 4%).

comparison of the spectra indicates that, in spite of the hematite segregation, the Fe:TiO_2 samples must also contain iron inserted as dopant in the titania lattice. The band gap can be estimated from the UV–vis DRS considering the variation of semiconductor absorption (α) with the incident photon energy ($h\nu$), employing a modified Kubelka–Munk function.[30] For the direct-allowed electronic transition, the region near the absorption edge $(\alpha h\nu)^2$ exhibited a linear relationship with $h\nu$ (inset in Figure 4), and E_{BG} can be determined by extrapolation of the intercept with the abscissa. The E_{BG} for TiO_2 was estimated as 3.2 eV, which is in good agreement with the reported values for anatase phase.[38] For Fe:TiO_2, the E_{BG} values decreased from 3.0 to 2.7 eV for samples with the relative Fe/Ti amount increasing from 1 to 5%.

The annealed powder samples were also investigated by EXAFS measurements. Comparison of the X-ray absorption near-edge spectra (XANES) obtained for these samples (see Figure S3 in the Supporting Information) revealed that the main edge crest, observed at 4976 eV, was not altered by iron content. Also, all the spectra exhibited similar features; peaks at ca. 4987 and 5002 eV, and a peak at pre-edge (from 4965 to 4975 eV), which can be attributed to transitions from Ti 1s to 3d energy levels. The Fe K-edge XANES spectra also exhibited similar features for all samples, with the main peak observed at 7119 eV.[39,40]

The EXAFS oscillations and their corresponding FT (performed with k^2-weighted) of the data for titania, hematite, Fe:TiO_2 and the mixture hematite/titania are shown in Figure 6. For the Ti K-edge, Figure 6a, b, similar spectra were obtained for all the samples. Independent of Fe content, the EXAFS oscillations remained unchanged; all the FT curves exhibit the main peaks at equivalent distances and with similar magnitude. The radial distribution function around the absorbing atom (FT curves) can be discussed considering the anatase and brookite structure (see Figure S4 in the Supporting Information); in the first one titanium is coordinated with six oxygen atoms, with four neighbors at 1.98 Å and other two at 1.93 Å.[41] Brookite shows a similar structure, titanium being coordinated with six oxygen atoms, located at different distances, ranging from 1.86 to 2.04 Å. The distances were obtained from the structure used in the refinement.[42] Because of the similar distances between titanium and oxygen atoms in anatase and brookite the interpretation of the spectra can be carried out considering both as scattering the same signal, although the contribution of brookite should be smaller due to its smaller mass percentages in the samples. Thus, the main FT maximum at Figure 6b can be associated with the nearest shell around the absorbing Ti atom, consisting of six O neighbors; the second maximum can be related to the four Ti atoms and the next peak to the third coordination shell of O atoms which is similar in brookite and anatase. Therefore, the distances for these coordination shells for Fe:TiO_2 samples are similar to those exhibited by TiO_2.

For hematite, a distorted octahedral configuration is also found; around iron, there are three oxygen atoms at 1,94 Å and other three at 2.12 Å.[17] For data obtained at the Fe K-edge (Figure 6d), the first FT maximum for hematite can be attributed to six nearest oxygen neighbors; the second peak, with similar or higher magnitude, has been associated to superposed contributions of Fe and O shells.[43] For Fe:TiO_2 samples, however, the first maximum is much higher than the second one, suggesting that the second coordination shell for Fe:TiO_2 samples is different from that for hematite. This feature was interpreted as an indication that absorbing Fe occupied a Ti site at TiO_2 lattice. As observed in Figure 6d, the features after the first peak in Fe K-edge show an evolution with the increasing iron content in the samples, having a similar shape to that observed for α-Fe_2O_3/TiO_2 samples. This behavior is indicative that the observed spectra are scattered by Fe atoms in TiO_2 lattices as well as in α-Fe_2O_3 lattices, and the contribution of α-Fe_2O_3 is increasing with the iron mass percentage in Fe:TiO_2 samples. Thus, the higher the initial Fe concentration, the higher the amount of segregated hematite, which is consistent with the Rietveld refinement of the XRD data.

Probably, hematite segregated at grain boundaries of the Fe:TiO_2 particles and, due to the low relative concentration, could not be identified by EXAFS. This hypothesis is supported by comparison of bright field TEM images and elemental mapping obtained for α-Fe_2O_3/TiO_2 (Fe/Ti = 4%) and

Fe:TiO_2(5%) samples at Figure 7. The insets in b and d in Figure 7 exhibit the iron signal (721 eV) in EELS spectra; for

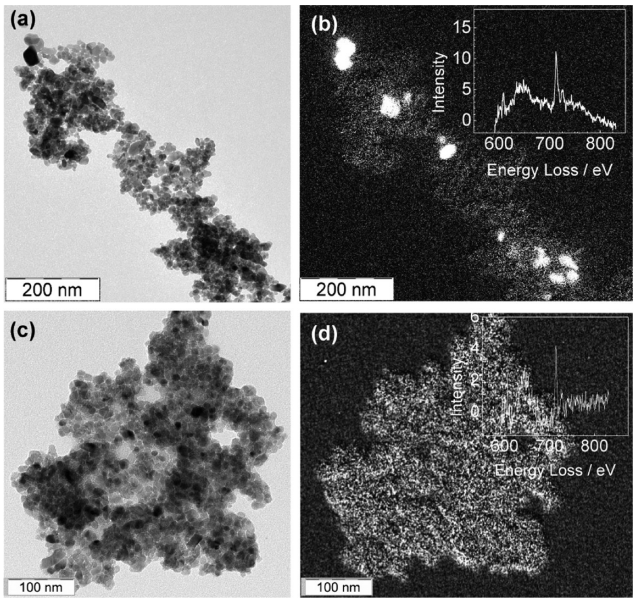

Figure 7. TEM bright-field images and elemental mapping (Inset: EELS spectra) for (a, b) a mixture of the α-Fe_2O_3/TiO_2 (4%) and (c, d) Fe:TiO_2 (5%).

the hematite/titania mixture the elemental mapping revealed regions with accumulated iron (brighter dots, Figure 7b), which can be associated with hematite particles in the sample. For the Fe:TiO_2(5%) sample (Figure 7d), iron is also identified but it must be homogeneously distributed and hematite particles cannot be recognized in the image, suggesting that hematite can be segregated at the grain boundaries of Fe:TiO_2 particles.

The presence of segregated hematite in the Fe:TiO_2 grain boundaries can affect the separation of photogenerated charges (electron/hole pair), as well as the electron transport through a Fe:TiO_2 film, when this material is used as photocatalyst, considering the differences in dielectric constants for TiO_2 and α-Fe_2O_3. The dielectric constant values for anatase and hematite, estimated at 298−300 K, correspond to 55 and 12, respectively.[25,44] In fact, we are also investigating the photoelectrochemical properties of thin films of TiO_2 and Fe:TiO_2 and a worse performance has been observed for Fe:TiO_2 (these results will be published later). Thus, the controversial results observed in literature for the performance of Fe:TiO_2 particles (or films) as photocatalyst for solar energy conversion can be probably related to an eventual segregation of hematite.

4. CONCLUSIONS

Nanosized particles of crystalline TiO_2, α-Fe_2O_3, and iron-doped TiO_2 (Fe:TiO_2) were synthesized by the sol−gel method (with Fe/Ti molar ratio corresponding to 1, 3 and 5%), followed by hydrothermal treatment, drying and annealing. Rietveld refinement of the X-ray diffraction data revealed that TiO_2 consisted of 82% anatase and 18% brookite; for Fe:TiO_2, the brookite contribution was higher than 30%. Since hematite was also identified in all of the Fe:TiO_2 samples (0.5, 1.0, and 1.2 wt % for samples prepared with 1; 3 and 5% of Fe/Ti), their characteristics were compared to a mixture consisting of hematite/titania (with 4% of Fe/Ti). Considering that the band gap energy, estimated as 3.2 eV for TiO_2, gradually ranged from 3.0 to 2.7 eV with increasing Fe content in the Fe:TiO_2 samples, it can be assumed that a Fe fraction was also inserted as dopant in TiO_2. Furthermore, because the lattice parameters and unit cell volume for brookite were more affected than for anatase, it can be inferred that iron could be preferentially inserted into the brookite crystallographic phase. However, since hematite features were not identified by extended X-ray absorption fine structure spectra, neither in the images obtained by transmission electron microscopy, probably hematite was segregated at the grain boundaries of Fe:TiO_2. Considering that α-Fe_2O_3 exhibits a much lower dielectric constant than TiO_2, its presence at the grain boundaries will hinder the separation of photogenerated charges, affecting significantly the material performance as a photocatalyst for solar energy conversion.

■ ASSOCIATED CONTENT

Supporting Information

Procedures of samples preparation for ICP OES analysis, XRD patterns obtained in different stages of synthesis, progression of lattice parameters and unit cell volumes for crystallographic anatase and brookite phases, XANES spectra obtained at Ti- and Fe−K edges, and anatase structure. This material is available free of charge via the Internet at http://pubs.acs.org.

■ AUTHOR INFORMATION

Corresponding Author

*E-mail: clalongo@iqm.unicamp.br; +55 19 3521 3411.

Notes

The authors declare no competing financial interest.

■ ACKNOWLEDGMENTS

The assistance of Ana Paula Sotero, Daniela Zanchet, and Roy Edward Bruns are gratefully acknowledged. This work was supported by CAPES, CNPq, FAPESP, National Institute of Science, Technology and Innovation on Advanced Complex Materials (INOMAT), and National Institute of Science and Technology for Bioanalytics (INCTBio).

■ REFERENCES

(1) Chen, X.; Mao, S. S. *Chem. Rev.* **2007**, *107*, 2891.
(2) Grätzel, M. *Photochem. Photobiol. C* **2003**, *4*, 145.
(3) Longo, C.; De Paoli, M.-A. *J. Braz. Chem. Soc.* **2003**, *14*, 889.
(4) Hagfeldt, A.; Boschloo, G.; Sun, L.; Kloo, L.; Pettersson, H. *Chem. Rev.* **2010**, *110*, 6595.
(5) Liu, Z.; Li, Y.; Li, C.; Ya, J.; Lei, E.; Zhao, W.; Zhao, D.; Na, L. *ACS Appl. Mater. Interfaces* **2011**, *3*, 1721.
(6) Lee, H.; Hwang, D.; Jo, S. M.; Kim, D.; Seo, Y.; Kim, D. Y. *ACS Appl. Mater. Interfaces* **2012**, *4*, 3308.
(7) Walter, M. G.; Warren, E. L.; McKone, J. R.; Boettcher, S. W.; Mi, Q.; Santori, E. A.; Lewis, N. S. *Chem. Rev.* **2010**, *110*, 6446.
(8) Fujishima, A.; Zhang, X.; Tryk, D. A. *Surf. Sci. Rep.* **2008**, *63*, 515.
(9) Oliveira, H. G.; Nery, D. C.; Longo, C. *Appl. Catal., B* **2010**, *93*, 205.
(10) Akpan, U. G.; Hameed, B. H. *Appl. Catal., A* **2010**, *375*, 1.
(11) Asahi, R.; Morikawa, T.; Ohwaki, T.; Aoki, K.; Taga, Y. *Science* **2001**, 269.
(12) Choi, J.; Park., H.; Hoffmann., M. *J. Phys. Chem. C* **2010**, *114*, 783.
(13) Kachina, A.; Puzenat, E.; Ould-Chikh, S.; Geantet, C.; Delichere, P.; Afanasiev, P. *Chem. Mater.* **2012**, *24*, 636.
(14) Zhang, J.; Pan, C.; Fang, P.; Wei, J.; Xiong, R. *ACS Appl. Mater. Interfaces* **2010**, *2*, 1173.

(15) Liu, H.; Wu, Y.; Zhang, J. *ACS Appl. Mater. Interfaces* **2011**, *3*, 1757.
(16) Pulsipher, D. I.; Martin, I. T.; Fisher, E. R. *ACS Appl. Mater. Interfaces* **2010**, *2*, 1743.
(17) Zhu, S.; Shi, T.; Liu, W.; Wei, S.; Xie, Y.; Fan, C.; Li, Y. *Phys. B* **2007**, *396*, 177.
(18) Qingping, W.; van de Krol, R. *J. Am. Chem. Soc.* **2012**, *134*, 9369.
(19) Wang, X. H.; Li, J.-G.; Kamiyama, H.; Moriyoshi, Y.; Ishigaki, T. *J. Phys Chem B* **2006**, *110*, 6804.
(20) Santos, R. S.; Oliveira, H. G.; Longo, C. In *Proceedings of SPIE: Solar Hydrogen and Nanotechnology IV*; Osterloh, F. E., Ed.; International Society for Optics and Photonics: Bellingham, WA, 2009; Vol. *7408*, p 74080O.
(21) Sonawane, R. S.; Kale, B. B.; Dongare, M. K. *Mater. Chem. Phys.* **2004**, *85*, 52.
(22) Piera, E.; Tejedor-Tejedor, M. I.; Zorn, M. E.; Anderson, M. A. *Appl. Catal., B* **2003**, *46*, 671.
(23) Colemenares, J. C.; Aramendia, M. A.; Marinas, A.; Marinas, A.; Urbano, F. *J. Appl. Catal. A* **2006**, *306*, 120.
(24) Yang, M.; Hume, C.; Lee, S.; Son, Y. H.; Lee, J. K. *J. Phys. Chem. C* **2010**, *114*, 15292.
(25) Young, K. F.; Frederikse, H. P. R. *J. Phys. Chem. Ref. Data* **1973**, *2*, 313.
(26) Wang, J. A.; Limas-Ballesteros, R.; Lopez, T.; Moreno, A.; Gomez, R.; Novaro, O.; Bokhimi, X. *J. Phys. Chem. B* **2001**, *105*, 9692.
(27) Litter, M. I.; Navío, J. A. *J. Phochem. Photobiol. A* **1996**, *98*, 171.
(28) Li, X.; Yue, P. L.; Kutal, C. *New J. Chem.* **2003**, *27*, 1264.
(29) Huo, L.; Li, Q.; Zhao, H.; Yu, L.; Gao, S.; Zhao, J. *Sens. Actuators B* **2005**, *107*, 915.
(30) Wang, X. H.; Li, J.-G.; Kamiyama, H.; Katada, M.; Ohashi, N.; Moriyoshi, Y.; Ishigaki, T. *J. Am. Chem. Soc.* **2005**, *127*, 10982.
(31) Larson, A. C.; Von Dreele, R. B. *LANL Report LAUR 86-748: General Structure Analysis System (GSAS)*; Los Alamos National Laboratory: Los Alamos, NM, 1994.
(32) Toby, B. H. *J. Appl. Crystallogr.* **2001**, *34*, 210.
(33) Bokimi, X.; Morales, A.; Novaro, O.; Lopéz, T.; Gomez, R. *J. Mater. Res.* **1995**, *10*, 2788.
(34) Young, R. A. In *The Rietveld Method*; Oxford University Press: New York, 1993.
(35) Azimov, P. Y.; Bushmin, S. A. *Geochem. Int.* **2007**, *45*, 1210.
(36) Shannon, R. D. *Acta Crystallogr.* **1976**, *32*, 751.
(37) Colon, G.; Hidalgo, M. C.; Munuera, G.; Ferino, I.; Cutrufello, M. G.; Navio, J. A. *Appl. Catal., B* **2006**, *63*, 45.
(38) Ambrus, Z.; Balázs, N.; Alapi, T.; Wittmann, G.; Sipos, P.; Dombi, A.; Mogyorósi, K. *Appl. Catal., B* **2008**, *81*, 27.
(39) Farges, F.; Bronw, G. E.; Rehr, J. *J. Phys. Rev. B* **1997**, *56*, 1809.
(40) Angelomé, P. A.; Andrini, L.; Calvo, M. E.; Requejo, F. G.; Bilmes, S. A.; Soler-Illia, G. J. A. A. *J. Phys. Chem. C* **2007**, *111*, 10886.
(41) Vasiliu, F.; Diamandescu, L.; Macovei, D.; Teodorescu, C. M.; Nicula, R. *J. Mater. Sci: Mater. Electron* **2009**, *20*, 211.
(42) Djerdj, I.; Tonejc, A. M. *J. Alloys Compd.* **2006**, *413*, 159.
(43) Diamandescu, L.; Vasiliu, F.; Tarabasanu-Mihaila, D.; Feder, M.; Vlaicu, A. M.; Teodorescu, C. M.; Macovei, D.; Enculescu, I.; Parvulescu, V.; Vasile, E. *Mater. Chem. Phys.* **2008**, *112*, 146.
(44) Carp, O.; Huisman, C. L.; Reller, A. *Prog. Solid State Chem.* **2004**, *32*, 33.